Manganese Limitation of Phytoplankton Physiology and Productivity in the Southern Ocean

Nicholas J. Hawco[1]†, Alessandro Tagliabue[2]†, and Benjamin S. Twining[3]

[1] Department of Oceanography, University of Hawai'i at Mānoa; Honolulu, HI, USA.

[2] School of Environmental Sciences, University of Liverpool; Liverpool, UK.

[3] Bigelow Laboratory for Ocean Sciences; East Boothbay Maine, USA.

Corresponding authors: Nicholas Hawco (hawco@hawaii.edu) and Alessandro Tagliabue: (a.tagliabue@liverpool.ac.uk)

† These authors contributed equally to this work

Key Points:

- Mn scarcity in the Southern Ocean limits phytoplankton growth in a global biogeochemical model, especially during austral spring.
- The spatial extent of Mn limitation is sensitive to phytoplankton traits governing photophysiology and metal homeostasis.
- Greater dust deposition to the Southern Ocean expands the role of Mn limitation and restricts carbon export resulting from Fe fertilization.

Abstract

Although iron and light are understood to regulate the Southern Ocean biological carbon pump, observations have also indicated a possible role for manganese. Low concentrations in Southern Ocean surface waters suggest manganese limitation is possible, but its spatial extent remains poorly constrained and direct manganese limitation of the marine carbon cycle has been neglected by ocean models. Here, using available observations, we develop a new global biogeochemical model and find that phytoplankton in over half of the Southern Ocean cannot attain maximal growth rates because of manganese deficiency. Manganese limitation is most extensive in austral spring and depends on phytoplankton traits related to the size of photosynthetic antennae and the inhibition of manganese uptake by high zinc in Antarctic waters. Importantly, manganese limitation expands under the increased iron supply of past glacial periods, reducing the response of the biological carbon pump. Overall, these model experiments describe a mosaic of controls on Southern Ocean productivity that emerge from the interplay of light, iron, manganese and zinc, shaping the evolution of Antarctic phytoplankton since the opening of the Drake Passage.

Plain Language Summary

Because of the Southern Ocean's unique role in ocean circulation, Antarctic phytoplankton profoundly influence the global carbon cycle. For instance, an increase in the supply of iron – the main nutrient limiting Antarctic phytoplankton – is thought to have lowered CO_2 during past ice ages by increasing phytoplankton photosynthesis. However, the potential for other essential elements to limit Southern Ocean productivity is not well known. By accounting for requirements of several nutrients in a global model, we have identified that manganese, an essential cofactor in photosynthesis, can limit phytoplankton growth across the Southern Ocean. The enduring role of manganese deficiency will likely influence the response of Southern Ocean ecosystems to ongoing climate change.

1 Introduction

The persistent outgassing of CO_2 from the Southern Ocean to the atmosphere contributes to the warm interglacial climate of the Holocene (Sarmiento & Toggweiler, 1984; Sigman et al., 2010; Sigman & Boyle, 2000). South of the Polar Front, deep circumpolar water masses upwell into the surface mixed layer, ventilating the deep ocean carbon reservoir and enriching surface waters with high concentrations of the macronutrients nitrate, phosphate, and silicate (Martin, 1990; Sarmiento et al., 2004). Consumption of these macronutrients in support of phytoplankton carbon fixation and the export of biomass to the deep ocean by the biological carbon pump can

compensate for the leak of upwelled CO_2 out of the ocean (Sigman et al., 2010), but only if environmental conditions (light, temperature) permit growth and essential micronutrients, such as iron (Fe), are in sufficient supply (Martin et al., 1990; Martínez-García et al., 2014).

Outside of the light-limited period around winter, Fe is considered to be the major factor shaping phytoplankton growth in the Southern Ocean spring and summer (Boyd, 2002; Tagliabue et al., 2014). Phytoplankton primarily need Fe for their photosynthetic apparatus, especially photosystem I (PSI), which contains up to six-fold more Fe than photosystem II (PSII) (Raven, 1990; Strzepek & Harrison, 2004). Accordingly, phytoplankton tend to adapt to Fe limitation with elevated PSII:PSI ratios, which economizes Fe use (Strzepek & Harrison, 2004) (although this response is surprisingly muted in Southern Ocean lineages (Strzepek et al., 2019)). The primary production that underpins Southern Ocean ecosystems relies on deep winter mixing to supply dissolved iron (dFe) to the euphotic zone, supplemented by additional sources from dust, continental margins and the cryosphere (Tagliabue et al., 2014, 2017). In this context, increases in iron supply from dust during glacial periods is postulated to alleviate phytoplankton Fe limitation, enhancing both macronutrient utilisation and carbon export in the Southern Ocean and reducing atmospheric CO_2 (Jaccard et al., 2013; Martin, 1990; Martínez-García et al., 2014; Sigman et al., 2010).

The use of Fe in the photosynthetic apparatus occurs alongside manganese (Mn), an essential component of the Mn_4O_5Ca oxygen-evolving complex of photosystem II (Raven, 1990). Phytoplankton Mn requirements are also driven by use of Mn as a cofactor in superoxide dismutase, arginase, and other metalloenzymes (Peers & Price, 2004; Twining & Baines, 2013), but uptake of Mn from seawater is complicated by the poor selectivity of phytoplankton metal transporters for Mn^{2+} in the presence of similar concentrations of Zn^{2+}, Cu^{2+}, and Cd^{2+} (Sunda &

Huntsman, 1996, 1998b, 2000). This is consistent with predictions from the Irving-Williams Series, the periodic trend of increasing divalent metal-binding affinity of organic molecules following the order $Mn^{2+} < Fe^{2+} < Co^{2+} < Ni^{2+} < Cu^{2+} > Zn^{2+}$ (Irving & Williams, 1953), which shapes metal metabolism and physiology in all domains of life (Waldron & Robinson, 2009). Below the euphotic zone, heterotrophic bacteria oxidize soluble Mn^{2+} to insoluble Mn(III/IV) oxides, which accumulate in seafloor sediments (Johnson et al., 1996; Sunda & Huntsman, 1988), leading to low dissolved Mn (dMn, ~ 0.3 nM) at depth compared to concentrations of 1–5 nM found in the surface of oligotrophic gyres (Boyle et al., 2005; Hatta et al., 2015; Hulten et al., 2017; Johnson et al., 1996; Landing & Bruland, 1987).

Mn-poor water masses in the deep ocean are primarily ventilated in the Southern Ocean. Relative to other Fe-limited regions where Mn supply is greater, the first reports of dMn in the Southern Ocean emphasized unusually low concentrations, proposing the potential for Mn co-limitation alongside Fe (Martin et al., 1990). More recent surveys have confirmed that dMn in both the Antarctic and Subantarctic zones can be < 0.05 nM, the lowest measured globally (Browning et al., 2014; Latour et al., 2021; Middag et al., 2011, 2013). The Antarctic Zone south of the Polar Front also features Zn^{2+} concentrations that are 100 to 1000 fold higher than temperate and tropical regions (Baars & Croot, 2011), which should depress algal Mn uptake via competition for membrane transporters. Indeed, recent experiments have indicated that Mn can be the primary limiting nutrient to phytoplankton growth in the Drake Passage (Browning et al., 2021) and the Ross Sea (Wu et al., 2019), supporting prior suggestions of Mn limitation in the Southern Ocean (Browning et al., 2014; Buma et al., 1991; Martin et al., 1990). Despite this emerging evidence, the scale of Mn limitation across the Southern Ocean is undefined. Global models that have appraised Mn cycling have not considered growth limitation terms (Hulten et

al., 2017; Richon & Tagliabue, 2021) and simple, observation-based models that advocate for the possibility for Mn limitation in this region (Browning et al., 2021; Moore, 2016) have not accounted for the interplay of ocean circulation and mixing, phytoplankton physiology, and metal sources, sinks, and recycling pathways needed to simulate Southern Ocean biogeochemistry in an integrated manner. Overall, this limits our understanding of how Mn scarcity may impact phytoplankton growth and the strength of the biological carbon pump at large scales, particularly during fluctuations in Fe supply across seasons or during past or future changes in climate.

Here, we incorporate phytoplankton Mn uptake and Mn requirements into a coupled global ocean physics-biogeochemistry model to assess the global impact of Mn limitation for the first time. Our simulations explicitly represent a range of mechanistic processes, including external inputs and internal cycling of Mn, alongside the biogeochemical cycles of carbon, nitrogen, phosphorus, silicon, and iron. Our model results highlight a widespread impact of Mn on phytoplankton growth that is most intense during the austral spring and underpinned by key phytoplankton traits governing light and resource acquisition. Moreover, additional simulations using reconstructions of dust supply of both Fe and Mn during the Last Glacial Maximum period demonstrate how the scale of Mn limitation is sufficient to impact the response of Southern Ocean productivity and the carbon cycle. Ultimately, relief of Fe limitation in the Southern Ocean is compensated by an expansion of Mn limitation, an interplay that has likely driven the evolution of polar phytoplankton over millions of years.

2 Materials and Methods

2.1 Biogeochemical cycles of Zn and Mn in the PISCES-BYONIC model

The PISCES-BYONIC model is based on PISCES-v2 (Aumont et al., 2015), with the

addition of global cycles of the micronutrients Mn, Zn, Cu and Co (Hulten et al., 2017; Richon & Tagliabue, 2019, 2021; Tagliabue et al., 2018). The Fe cycle in PISCES-v2 has also been modified to allow regulation reducing Fe uptake rate in nitrogen-limiting conditions, consistent with recent measurements (Twining et al., 2020). This study adds equations representing phytoplankton Mn uptake and Mn growth requirements to the PISCES-BYONIC model. The modifications are described in detal below. Full details of the PISCES-v2 model can be found in Aumont et al. (Aumont et al., 2015) and equations governing the Mn and Zn biogeochemical cycles are fully described in the Supplementary Information of Richon and Tagliabue (Richon & Tagliabue, 2021). Briefly, the Mn model accounts for sources of Mn from atmospheric deposition, rivers, marine sediments, and hydrothermal vents. Mn in dust is assumed to be 25% soluble and the sediment supply is enhanced at both low oxygen and at higher organic carbon flux. In the model, Mn is removed from the ocean by bacterially-catalyzed precipitation of Mn oxides, which sink to the seafloor. Rates of bacterial scavenging of dMn increase with increasing temperature (Richon & Tagliabue, 2021; Tagliabue et al., 2018) but decrease when dMn falls below a threshold concentration, which is important for replicating the residual dMn inventory in the deep ocean (Hulten et al., 2017). High light and low oxygen also decrease the rate of Mn scavenging and enable the dissolution of Mn oxides, most notably in the illuminated surface mixed layer and in low oxygen water masses in the tropics, respectively. Compared to Mn, the Zn cycle in the model is less influenced by external sources (dust and riverine input) and more by internal recycling mechanisms, including biological uptake and regeneration, as well as reversible scavenging onto particulate organic carbon (Weber et al., 2018). Bioavailable Zn is calculated by equilibrium with a single ligand at a fixed concentration of 1 nM. A small fraction of Zn uptake is also allocated to diatom frustules, and cycles in parallel to Si in the model

147 (Weber et al., 2018). Modelled Mn and Zn cycles in PISCES-BYONIC reproduce the major
148 features of their oceanic distributions (Richon & Tagliabue, 2021; see also Figs. S1, S2).

149 **2.2 The minimum Mn requirement**

150 Minimum phytoplankton requirements for Mn are defined by a manganese use efficiency
151 (MnUE), whereby increasing Mn is needed to support increasing growth rates (Raven, 1990).
152 The MnUE represents the rate that carbon biomass can be produced per catalytic Mn atom,
153 having units of mol C day^{-1} (mol Mn)$^{-1}$, and is described by:

154 $$MnUE_i = \frac{\mu_i}{Q_{Mn,Req}} \quad (1)$$

155 Where μ is the specific growth rate (day^{-1}) and $Q_{Mn,Req}$ is the required quota, the amount needed
156 to power photosynthesis and basal metabolism (units of mol Mn (mol C)$^{-1}$). The subscript *i*
157 reflects separate calculations for diatom and nanophytoplankton functional types in the model.
158 $Q_{Mn,Req}$ is calculated as:

159 $$Q_{Mn,Req} = Q_{Mn,min} + 4 * \frac{Chl:C}{Chl:PSII} \quad (2)$$

160 Approximating growth of the cultured open ocean diatom *Thalassiosira oceanica* (Sunda, 1989;
161 Sunda & Huntsman, 1983, 1986), $Q_{Mn,min}$ is set to 1 μmol Mn : mol C at a reference growth rate
162 of 1 day^{-1}, equal to an MnUE of 10^6 mol C (mol Mn)$^{-1}$ day^{-1}; see Table 1. Conceptually this basal
163 requirement accounts for Mn metalloenzymes such as Mn superoxide dismutase, arginase,
164 carbonic anhydrase, among others (Jensen et al., 2019; McCain et al., 2021; Peers & Price, 2004;
165 Twining & Baines, 2013). While it is likely that each of these Mn enzymes are uniquely
166 regulated based on intracellular or extracellular conditions, the scope and extent of this
167 regulation is poorly defined at present. We consider the constant non-photosynthetic Mn
168 requirement to be a relatively conservative approach that appears consistent with the observation
169 of increasing Mn requirements with increasing growth rate described by Sunda and Huntsman

(Sunda & Huntsman, 1998b), as well as more general theories of nutrient limitation (Droop, 1973; Raven, 1988).

Table 1. Model parameters added to the PISCES-BYONIC model for this study. The parameter values are assigned following laboratory and field observations where possible. Parameters describing the Mn sources and sinks can be found in Richon and Tagliabue (2021)

Parameter	Value	Units	Description	Reference
$Q_{Mn,min}$	1.0	μmol mol^{-1}	Mn requirement not associated with photosynthesis	(Sunda, 1989; Sunda & Huntsman, 1986, 1996, 1998b)
Chl:PSII	1000	mol mol^{-1}	Photosynthetic antennae size	Table S1
$K_{Mn, nano}$ $K_{Mn, diatom}$	5×10^8 1.67×10^8	M^{-1}	Binding constant for Mn' to Mn transporter	(Sunda & Huntsman, 2000)
$K_{Zn,a}$	5×10^8	M^{-1}	Binding constant for Zn' to Mn transporter	(Sunda & Huntsman, 2000)
$K_{Zn,b\ nano}$ $K_{Zn,b\ diatom}$	1×10^9 0.33×10^9	M^{-1}	Binding constant for Zn' to the high affinity Zn transporter	(Sunda & Huntsman, 2000)
$Q'_{Mn,max}$	6	μmol mol^{-1}	Maximum Mn quota	SXRF Observations (Figure 2)
$Q'_{Zn,max,\ nano}$ $Q'_{Zn,max,\ diatom}$	30 40	μmol mol^{-1}	Maximum Zn quota	SXRF Observations (Figure 2)

The photosynthetic component of the Mn requirement is dictated by a dynamic chlorophyll scheme already simulated in PISCES-v2 (Aumont et al., 2015), originally based on the photoacclimation model of Geider et al. (1997). The Mn quota associated with PSII is calculated from the simulated Chl : C ratio by applying a fixed antennae size, represented as a Chlorophyll : PSII ratio (Chl : PSII), and a stoichiometry of 4 Mn atoms per PSII (Raven, 1990). The standard model uses a Chl : PSII ratio of 1000 to simulate the global characteristics of diatom and nanophytoplankton functional types. This value is in the upper end of the range of both field and culture observations (Table S1), with the exception of recent characterizations of Southern Ocean phytoplankton (Strzepek et al., 2019). It should be noted that phytoplankton Fe limitation can lead to an uncoupling of the Chl antennae from the photosynthetic apparatus, giving rise to large apparent Chl : PSII ratios that do not represent functional antennae-photosystem complexes (Behrenfeld & Milligan, 2013). This process is not included in the Chl parameterisation scheme, and thus we chose the intermediate Chl : PSII ratio of 1000 to reflect

the functional antennae size in the model. To ensure that this scheme was not overestimating Mn limitation for Southern Ocean phytoplankton, we calculated the Mn requirements inferred from the photo-physiological data of Strzepek et al. (2019) (Figure 1). PSII Use Efficiencies from that work (units: mol C (mol PSII) $^{-1}$ day^{-1}) were converted to Mn units via the Mn : PSII ratio (i.e. a value of 4). Averaging across the 3 Southern Ocean phytoplankton characterized in that study, grown at low irradiance under both low and high Fe availability, a relatively narrow range of photosynthetic Mn requirement is predicted: 2.85 ± 0.53 μmol Mn : mol C at a reference growth rate of 1 day^{-1} (note that, per Eq. 1, this value decreases as growth rate decreases). We compared this to our model by applying the maximum Chl : C ratio of the diatom functional type (0.05 g Chl (g C)$^{-1}$ or 673 μmol Chl : mol C, assuming a molar mass of 891 amu for chlorophyll *a* (Aumont et al., 2015)), the default antennae size of 1000, and the Mn:PSII ratio of 4. This calculation results in a photosynthetic Mn requirement equal to 2.69 μmol Mn : mol C (Fig. 1), within the range of expected photosynthetic Mn requirements calculated from Southern Ocean diatoms (Strzepek et al., 2019). Applying the larger Chl : PSII ratio of 2000, decreases this requirement to 1.35 μmol Mn : mol C, which appears to underestimate photosynthetic Mn requirements for these isolates (Fig. 1).

In the model, the MnUE constrains phytoplankton growth rate, calculated as:

$$\mu_{Mn,i} = MnUE_i * Q_{Mn,i} \quad (3)$$

where Q_{Mn} is the realized Mn:C ratio, set by dMn and other parameters influencing Mn uptake (see next section). Mn limitation of phytoplankton growth emerges when the Mn-constrained growth rate falls below the background growth rate (i.e. $\mu_{Mn} < \mu$), the latter governed by light, temperature, iron, nitrogen, phosphorus and silica (for diatoms). The overall strength of Mn-limitation (dimensionless) is:

$$lim_{Mn,i} = \min\left(1, \frac{\mu_{Mn,i}}{\mu_i}\right) \quad (4)$$

while a state of Mn-deficiency is analogously calculated as:

$$def_{Mn,i} = \min\left(1, \frac{\mu_{Mn,i}}{\mu_{light,i}}\right) \quad (5)$$

where the light-limited growth rate (μ_{light}) reflects growth when other potentially limiting nutrients, most notably Fe, are replete. The maximum required Mn quota associated with the light-limited growth rate, $Q_{MnReq,max}$, can be calculated by substitution into Eq. 1.

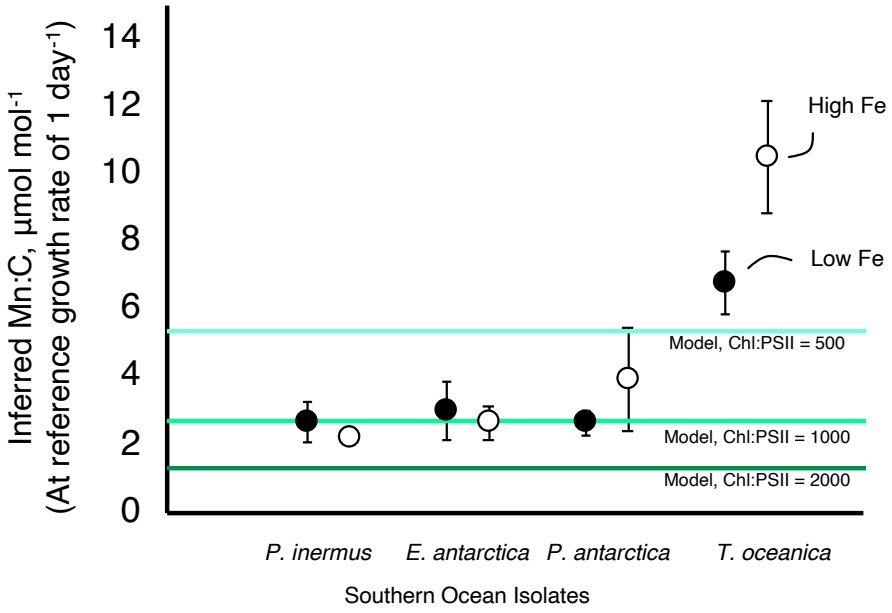

Figure 1. Estimated photosynthetic Mn:C requirements of three Southern Ocean phytoplankton isolates, the temperate diatom *T. oceanica*, and the diatom phytoplankton class in the PISCES-BYONIC model. Estimates from culture experiments are based on the PSII Use Efficiency of Strzepek et al. (2019), which were conducted under low-light conditions – where the photosynthetic apparatus is expected to be maximally upregulated – and under both high and low Fe availability (open and closed circles, respectively). The PSII Use Efficiency (units: mol C day^{-1} $(mol\ PSII)^{-1}$) is converted to Mn:C by applying 1) a reference growth rate of 1 day^{-1}, which normalizes across species-specific maximum growth rates, and 2) an Mn $PSII^{-1}$ stoichiometry of 4. Model values (horizontal lines) reflect maximally upregulated Chl:C for the diatom class (0.05 g g^{-1}) converted to Mn:C units with variable Chl : PSII ratios. This comparison suggests that the default Chl : PSII ratio of 1000 in the PISCES-BYONIC model is the best descriptor of these measurements, given the parametrization of Chl regulation, photosynthesis, and growth rates in the model. Note that higher reported Chl : PSII in Strzepek et al. (2019) (~2000:1) leads to a much higher Chl:C ratio than is simulated in the phytoplankton functional types represented in this global biogeochemical model.

2.2 Phytoplankton Mn uptake

Manganese uptake in both phytoplankton classes follows standard Michaelis-Menten kientics, modified to account for competetive inhibition due to Zn^{2+}.

$$\rho_{Mn,i} = V_{max,Mn} * \left(\frac{K_{Mn}[Mn']}{K_{Zn,a}[Zn']+K_{Mn}[Mn']+1}\right) \quad (6)$$

where K_{Mn} represents the equilibrium binding affinity of the manganese transporter to Mn and $K_{Zn,a}$ represents the affinity of Zn' to the same transporter. The maximum uptake rate, V_{max}, represents the number of transporter sites and a characteristic transport time. To reflect changes in the number of transporter sites, V_{max} is represented by the equation:

$$V_{max,Mn} = Q_{Mn\_max,i} * \mu_{max,i} * R_{up,Mn} * R_{down,Mn} * R_{Zn} \quad (7)$$

where a maximum uptake rate, defined as the product of the maximum quota, $Q_{Mn\_max,i}$, and the maximum growth rate is modulated by three physiological regulation terms: 1) R_{up}, transporter upregulation in response to low Q_{Mn}, 2) R_{down}, transporter downregulation in response to high Q_{Mn}, and 3) R_{Zn}, transporter downregulation in response to hyperaccumulation of internal Zn. Each of these behaviors have been observed in the open ocean diatom *T. oceanica* (Sunda & Huntsman, 1983, 1986, 2000), but corresponding experiments have not been performed for Antarctic species thus far. In the standard model, R_{Zn} is set equal to 1, which indicates no downregulation of Mn uptake in response to high Q_{Zn}. It is important to note that this confers an adaptive advantage to the modelled diatoms beyond that observed in *T. oceanica* and coastal species (Sunda & Huntsman, 1996, 1998a, 1998b, 2000). For simplicity, we have not accounted for similar competitive inhibition by Cu^{2+} and Cd^{2+} because concentrations of these ions in the Southern Ocean do not appear high enough to influence Mn uptake, in contrast to Zn^{2+} (Baars et al., 2014; Baars & Croot, 2011; Heller & Croot, 2015). We expect that this omission may slightly underestimate the impact of Mn limitation in the Antarctic zone.

The Mn maximum quota is adjusted from its prescribed value (Table 1) as a function of Mn requirements ($Q_{Mn,Req}$) and the fractional nitrogen limitation term (*Nlim;* range 0 – 1):

$$Q_{Mn\_max,i} = Q_{Mn,Req} + \left(Q'_{Mn\_max,i} - Q_{Mn,Req}\right) * Nlim \quad (8)$$

We note that this modification improves comparisons with Single Cell X-Ray Fluorescence (SXRF) measurements of Mn quotas, which are low in oligotrophic regions despite high dissolved Mn availability (Figures 2, S3). An equivalent change to $Q_{Fe\_max,i}$ is also implemented, which is also advocated by SXRF dataset (Twining et al., 2020).

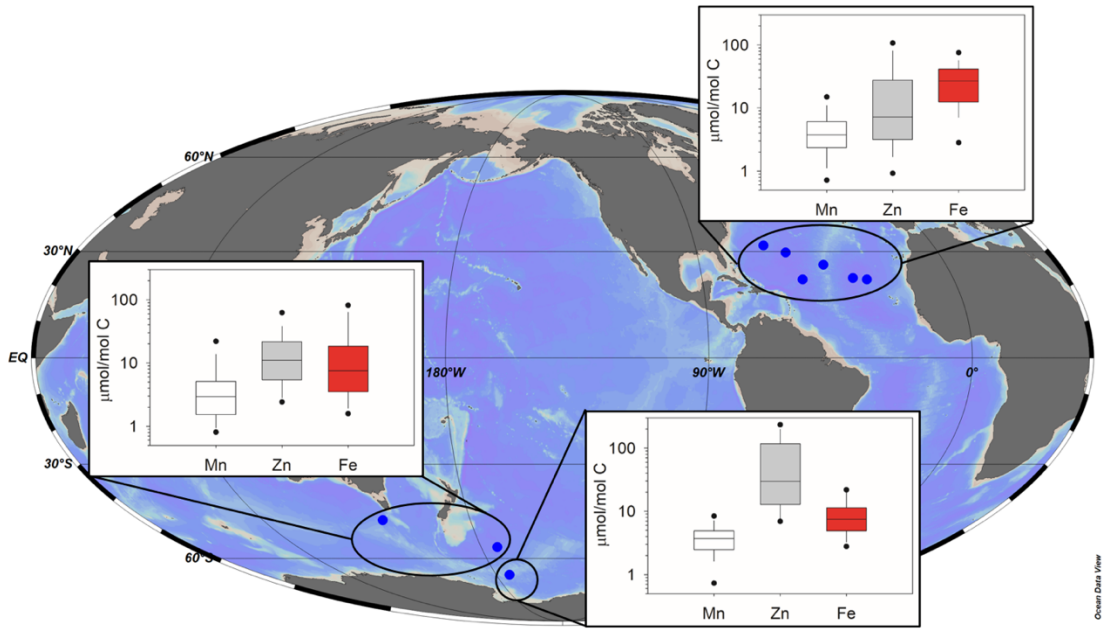

Figure 2. Comparison of phytoplankton Mn, Zn and Fe quotas from three oceanic regions measured by SXRF. For SXRF measurements, horizontal lines represent the dataset median value, box dimensions represent 25th and 75th quartiles, and whiskers cover the 10th and 90th percentiles. Black symbols indicate 5th and 95th percentiles. Data sources and number of cells analyzed are listed in Table S2.

The upregulation function, $R_{up,Mn}$, is defined, as for Fe in the original PISCES-v2 code:

$$R_{up} = 4 - 4.5\left(\frac{\min(1, lim_{Mn})}{0.5 + \min(1, lim_{Mn})}\right) \quad (9)$$

and permits a maximum 4-fold upregulation when growth is strongly limited by Mn. The down-regulation function, $R_{down,Mn}$, is parallels that for Fe in PISCES-v2:

$$R_{down} = \max\left(0, \frac{1 - f_{max,Mn}}{1.05 - f_{max,Mn}}\right) \quad (10)$$

where:

$$f_{max,Mn} = \frac{Q_{Mn,i}}{Q_{Mn\_max,i}} \quad (11)$$

So that the uptake rate decreases as the ratio of Q_{Mn} to the maximum quota, Q_{Mn_max}, approaches a value of 1, avoiding build-up of cellular Mn above Q_{Mn_max}.

The Zn downregulation effect, $R_{down,Zn,}$ is defined similarly to $R_{down,Mn}$, following the equation:

$$R_{Zn} = \max\left(0.1, \frac{1 - f_{max,Zn}}{1.05 - f_{max,Zn}}\right) \quad (12)$$

where:

$$f_{max,Zn} = \frac{Q_{Zn,i}}{Q_{Zn_{max},i}} \quad (13)$$

except that the minimum downregulation by R_{Zn} is set to 0.1 (instead of 0 for R_{down}), which avoids a complete shutdown of Mn uptake at high Zn^{2+}. Modelled Zn uptake is analogous to Mn, where uptake is proportional to Zn' according to Michalis Menten kinetics:

$$\rho_{Zn,i} = V_{max,Zn}\left(\frac{K_{Zn,b}[Zn']}{K_{Zn,b}[Zn']+1}\right) \quad (14)$$

and

$$V_{max,Zn} = Q_{Zn\_max,i} * \mu_{max,i} * R_{up,Zn} * R_{down,Zn} \quad (15)$$

with $R_{up,Zn}$ and $R_{down,Zn}$ defined specifically for Zn in the same way as for Mn (Eq. 9, 10). In addition, $Q_{Zn\_max,i}$ is also decreased under N limitation as for Mn and Fe (Eq. 8).

2.4 Model experiments

The standard version of the PISCES-BYONIC model presented here includes Mn growth limitation and accounts for the transporter competition between Mn and Zn. The standard model

297 was integrated for 500 years using climatological offline physics fields to allow quasi
298 equilibrium of the biogeochemical tracers. We then conducted a set of parallel sensitivity tests,
299 all initialised from the same initial state as the full model. The sensitivity tests were designed to
300 test how different assumptions about the capabilities of Southern Ocean phytoplankton affected
301 the role of Mn in shaping biogeochemical cycles, and include: (1) a 'no Mn limitation' run, in
302 which phytoplankton growth in the full model was not affected by Mn, (2) a 'no Zn transporter
303 interaction' run, where the transporter impact of Zn on Mn uptake was removed, (3) a 'Mn
304 downregulation by Zn hyperaccumulation' run, where down-regulation of Zn uptake due to Q_{Zn}
305 exceeding Q_{Zn_max} also down-regulated Mn transport (i.e. Eq. 12 was implemented), (4) a 'very
306 large photosynthetic antennae' run, where photosynthetic Mn requirements were derived
307 assuming a Chl : PSII ratio of 2000 and (5) a 'moderate photosynthetic antennae' run, where Mn
308 costs were derived assuming a Chl : PSII ratio of 500 (see Table S1). To assess how accounting
309 for Mn limitation affected the response of the Southern Ocean Biological Carbon Pump, we
310 conducted two additional experiments where the standard model and the 'no Mn limitation'
311 model were forced by increased dust input, characteristic of the Last Glacial Maximum (LGM)
312 perod, as described by Lambert et al. (2015). Accounting for LGM levels of dust input affected
313 the supply of both Fe and Mn.

314 **2.5 Single cell X-ray Fluorescence (SXRF)**

315 Carbon-normalized Mn, Fe, and Zn quotas of individual cells in Fig. 2 were compiled
316 from previously published studies in Antarctic and Subantarctic waters and the North Atlantic
317 Ocean (Twining, Baines, & Fisher, 2004; Twining, Baines, Fisher, et al., 2004). These data were
318 supplemented with new data for Subantarctic cells collected from the Southern Ocean Time
319 Series station (SOTS, 47˚S, 142˚E) in March 2018 during a cruise on the R/V Investigator

(cruise IN2018_v02; Sofen et al., In Revision). Cells were collected from 15–40 m between 7–18 March, 2018 (Table S2; Ellwood et al., 2020)). Fifty-nine cells were collected in total. North Atlantic data were supplemented with cells collected from two stations in the North Atlantic in summer 2017 during the ZIPLoC cruise (R/V James Cook, cruise JC150; Sofen et al., In Revision). Cells were collected from 40 m depth. SXRF sample collection and analysis followed previously published methods using stringent trace metal clean techniques (Twining et al., 2011).

Individual cells from plankton populations are known to exhibit significant intra-population variability (Bucci et al., 2012). Outliers were identified following Twining et al. (2019). Briefly, log-transformed C-normalized quotas were fit with an ANCOVA model (JMP, SAS) that included log(biovolume), station, and cell type (diatom or nanoflagellate) as effects. Individual quotas were removed from the dataset if the Jackknife distances of the Studentized residuals of this model were greater than 3. Approximately 1% of cell quotas in the dataset were removed through this process. Additionally, Zn or Fe quotas > 200 or >300 μmol (mol C)$^{-1}$, respectively, were deemed to be impacted by abiotic material based on known physiological ranges (Sunda & Huntsman, 1995a, 1995b) and were removed. This affected less than 5 measurements in the dataset.

3 Results

3.1 Modelling minimum and realized manganese quotas

To quantify the impact of Mn scarcity on the Southern Ocean biological carbon pump, we incorporated phytoplankton Mn limitation into the PISCES-BYONIC configuration of the global ocean biogeochemical model PISCES (Richon & Tagliabue, 2021). The PISCES-BYONIC model represents limitation of phytoplankton growth by five nutrients: nitrogen, phosphorus, silica (for diatoms), iron, and manganese, as well as light, and allows for variable

cell chlorophyll and micronutrient quotas. The PISCES-BYONIC model reproduces global patterns of dMn, dZn, and dFe from GEOTRACES observations (Figures 3a, S1 and S2), as well as other key biogeochemical properties (Richon & Tagliabue, 2021; Tagliabue et al., 2016).

Minimum cellular requirements for Mn (normalised to cell carbon: Q_{MnReq}) are represented in the model as the sum of the demand for oxygen-evolving complexes in PSII and a basal requirement of Mn enzymes rooted in central metabolism, which then increase with increasing growth rate as observed in both Fe fertilization experiments (Twining, Baines, & Fisher, 2004) and culture studies (Sunda & Huntsman, 1998b). Modelled values of Q_{MnReq} are lowest in the subtropical gyres, where growth rates are low, light is abundant and the photosynthetic apparatus is downregulated. Meanwhile, the stronger seasonality of irradiance and deeper mixed layers in the Southern Ocean, combined with episodes of fast growth during Austral spring, lead to a markedly greater Mn demand that peaks in the Subantarctic zone between 40–50°S (Figure 3b).

Mn uptake in the PISCES-BYONIC model is a function of bioavailable Mn^{2+} and Zn^{2+}, which compete for the same transporter following experimental constraints (Sunda & Huntsman, 1996, 1998b). The combination of low dMn and high dZn of waters upwelling into the Southern Ocean leads to a minimum in Q_{Mn} between 60–70°S (Figure 3c). Close to the Antarctic continent and downstream of large islands (e.g. the Kerguelen Plateau in the Indian Sector), Q_{Mn} increases due to Mn inputs from margin sediments. However, Mn input to some coastal areas – notably the Ross Sea – appears insufficient to yield maximum Q_{Mn}, which is consistent with recent reports of phytoplankton Mn-Fe co-limitation there (Wu et al., 2019).

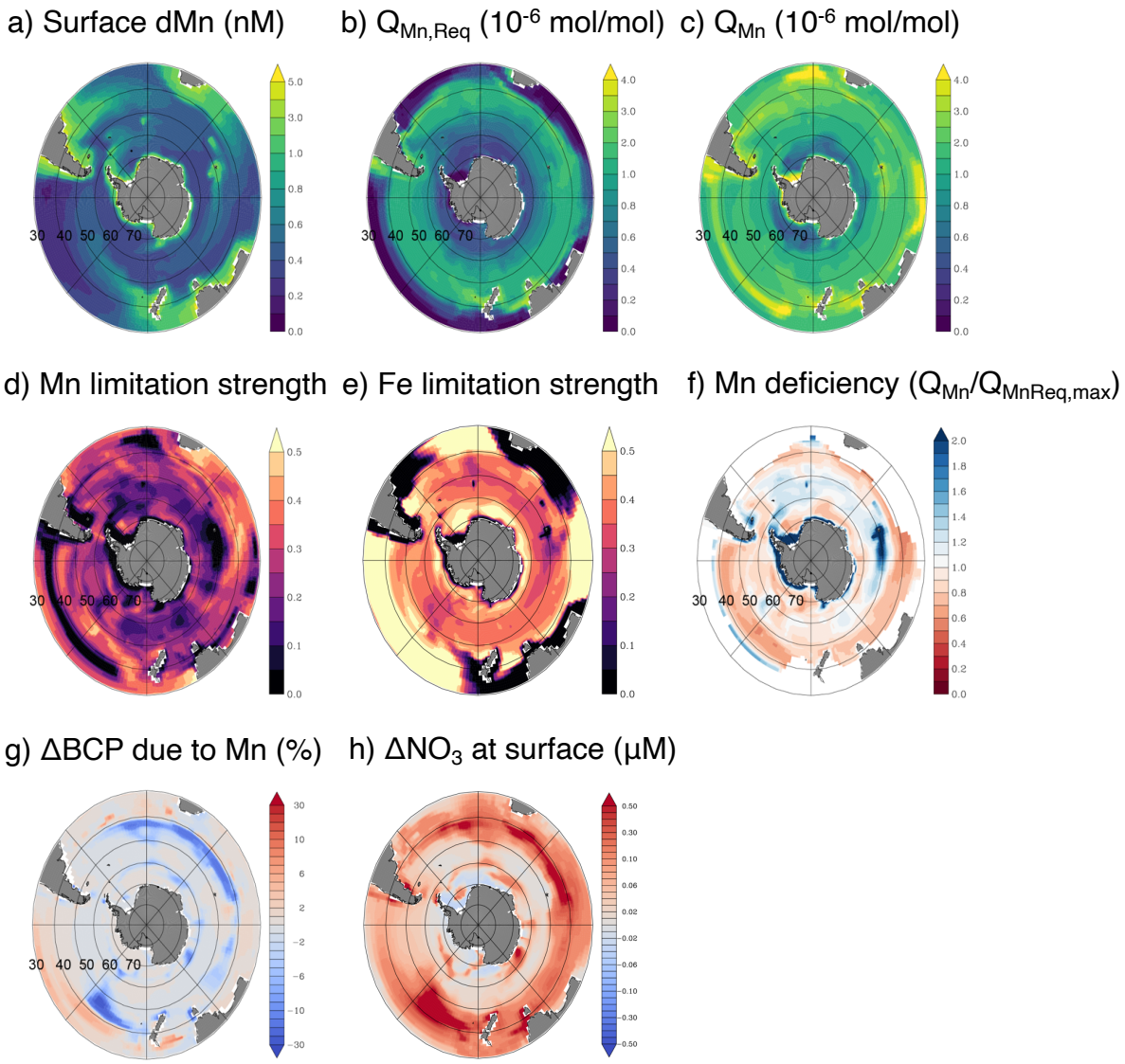

Figure 3. Southern Ocean manganese supply, demand, and limitation in PISCES-BYONIC. Factors influencing Mn uptake and use by Southern Ocean phytoplankton in January, including (a) dissolved Mn and (b) the minimum Mn requirement, Q_{MnREQ}, a function of phytoplankton chlorophyll and growth rate, normalized to biomass carbon. c) Mn uptake and phytoplankton growth rates dictate the Mn quota, Q_{Mn}. d) The Mn limitation term, derived as 1 – lim_{Mn} (see Eq. 4), where higher values indicate greater Mn limitation, and (e) the equivalent Fe limitation term. f) An index of Mn deficiency diagnosed from the ratio of Q_{Mn} to $Q_{MnREQ,max}$ (the Mn requirement associated with nutrient replete, light-limited growth rates). Panels a–c show January averages for the ocean surface, while d–f show seasonal minima. f) Relative to a control model without Mn feedbacks, Mn limitation decreases the biological carbon pump, BCP (defined at the 100 m depth horizon and integrated over the annual cycle), resulting in (h) an increase in the standing stock of nitrate at the ocean's surface.

3.2 Southern Ocean footprints of Mn limitation and Mn deficiency

Based on modelled Q_{Mn} and $Q_{Mn,Req}$, we calculated the proportion of maximum growth rate allowed by Mn (lim_{Mn}; Eq. 4) and subtracted this value from 1 to yield a unitless measure of 'Mn limitation' (Fig. 3d). Under this definition, higher values reflect more strongly Mn-limiting conditions. While large areas of the Southern Ocean are predicted to be 'Mn-limited' to some extent, the model simulated a greater prevalence and intensity of Fe limitation in the same regions (Fig. 3e), which is consistent with literature compilations of nutrient amendment experiments in the Southern Ocean (Table S3). Although Fe limitation is much more prevalent in our model, local pockets of Mn limitation reduce the strength of the biological carbon pump by up to 30% (Fig. 3g) with unused Fe and macronutrients fuelling a small increase in carbon export downstream. For context, this impact of Mn limitation on the biological carbon pump is similar to that of hydrothermal Fe supply (Resing et al., 2015; Tagliabue & Resing, 2016). In PISCES-BYONIC, the effects of Mn limitation are focused primarily in the Subantarctic between 40–50 ºS, especially in the Indian and Pacific sectors, with a smaller, patchier signal around 60 ºS (Fig. 3g). Ultimately, the reduced efficiency of macronutrient utilisation due to Mn limitation causes an increase in residual annual mean surface nitrate concentration (Fig. 3h), which is redistributed from the local sites of Mn limitation throughout the Southern Ocean by lateral mixing.

Beyond the small footprint for 'proximal' Mn limitation, we found that Q_{Mn} over most of the Southern Ocean did not strongly exceed Q_{MnReq} (Fig. 3b and c), indicating that Mn limitation might emerge rapidly with any increase in Fe supply. Indeed, the widespread Fe limitation typical of the Southern Ocean actually lowers Q_{MnReq} by enforcing slow growth rates. This indirect effect can be accounted for by defining a state of 'Mn deficiency,' which instead normalizes Q_{Mn} to the amount of Mn required to support growth rates in the absence of Fe limitation (i.e. $Q_{MnReq,max}$). Conceptually, this is similar to the additive responses observed in

bottle incubations where simultaneous addition of both Mn and Fe increase biomass more than Fe alone (Browning et al., 2021; Wu et al., 2019). In the standard version of the model, over half of the Southern Ocean experiences 'Mn deficiency' at some point during the seasonal cycle (62% of waters south of 40 ºS; Figure 3f).

3.3 *Seasonal phasing of Mn limitation*

The seasonal dynamics of ocean mixing across the Southern Ocean decouple the supply of Mn and Fe, leading to seasonal evolution of nutrient limitation regimes. Winter mixing supplies Fe from the ocean interior and is the dominant input of Fe across the Southern Ocean, with the wintertime Fe stock then recycled by marine ecosystems throughout the spring and summer (Boyd et al., 2012; Strzepek et al., 2005; Tagliabue et al., 2014). In contrast to Fe, entrainment by winter mixing does not elevate springtime mixed-layer Mn stocks notably, as concentrations in the ocean interior are also low (Latour et al., 2021; Moore, 2016; Rigby et al., 2020). As a result, localized Mn limitation can emerge as the Southern Ocean stratifies, primarily in November and December (Figure 4a, b), which hinders the progress of the austral spring bloom. During this period, Mn is more limiting than Fe in our model for 49% of Southern Ocean surface waters south of 40ºS. These waters are still characterized by low dFe concentrations, but the winter Fe supply that persists into spring permits relatively high growth rates while sub-optimal light levels also lead to elevated Chl, both of which increase Q_{MnReq}. By January and February, the mixed layer dFe reservoir is depleted, resulting in Fe limitation exceeding Mn limitation across 96% of the Southern Ocean south of 40ºS (Figure 4c). The ecosystem then returns to light limitation when mixed layers deepen in autumn (Figure 4d). This seasonal phasing between Mn and Fe limitation is not predicted from simpler models that do not account for variable Mn requirements (Browning et al., 2021), but it is key to allowing the mixed-layer

Fe stock to be repeatedly recycled and persist later into summer (Boyd et al., 2012; Strzepek et al., 2005). The seasonal progression from Mn to Fe limitation in the model is also consistent with the prevalence of Fe limitation from prior Fe and Mn addition experiments, which have mostly been conducted in austral summer (see Table S3).

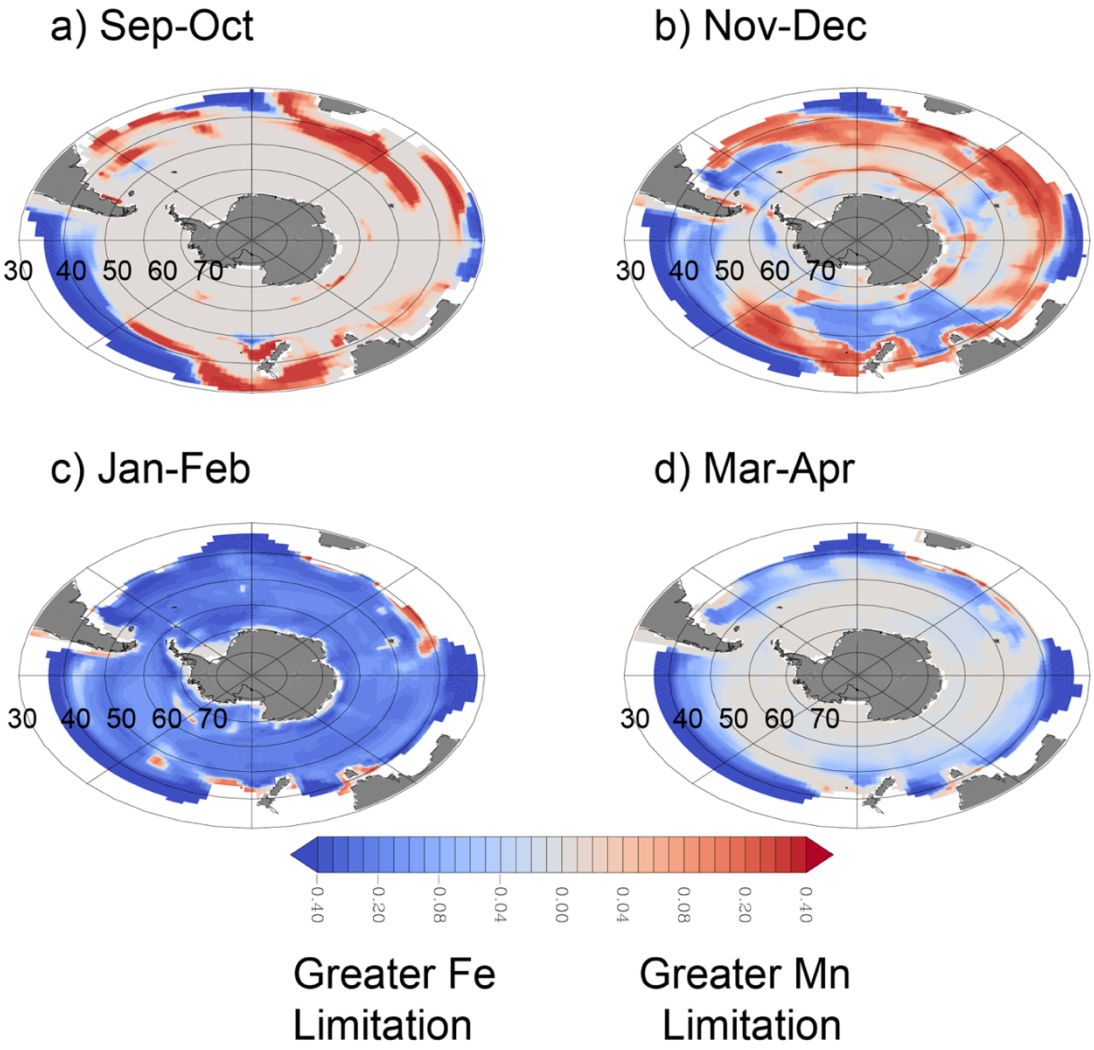

Figure 4. Seasonal phasing of Mn and Fe limitation. The difference between fractional Mn limitation and Fe limitation terms at the surface for (a) September–October, (b) November–December (c) January–February and (d) March–April. Positive values (in red) indicate greater Mn limitation than Fe limitation, while negative values indicate greater Fe limitation (blue). Nitrogen-limited areas at low latitudes are masked in white.

436 **3.4 *Seasonal phasing of Mn limitation***

437 Because the physiological characterization of important phytoplankton lineages is
438 incomplete (especially those from the Southern Ocean), we designed multiple sensitivity
439 experiments to examine how specific traits related to Mn uptake and use could affect the severity
440 of Mn limitation. When we removed Zn inhibition of Mn uptake, there was little change in the
441 Subantarctic zone biological carbon pump anomaly caused by Mn limitation, but the
442 corresponding anomaly in the Antarctic Zone was eliminated because Mn uptake in these high
443 Zn waters could now meet Mn requirements (Figure 5, S4). Conversely, if the Zn-Mn
444 antagonism is exacerbated by enabling the downregulation of Mn transport at high Q_{Zn}, a trait
445 that has been observed in culture experiments (Sunda & Huntsman, 1996, 2000), then the impact
446 of Mn limitation in the Antarctic zone is expanded greatly (Fig. 5). This effect would be further
447 increased if other divalent metals that compete for Mn transporters (Cu^{2+} and Cd^{2+}) were also
448 found to reach significant levels in the Antarctic zone. While traits related to Zn-Mn interactions
449 are crucial to the emergence of Mn limitation in the Antarctic Zone, the broad signal of Mn
450 limitation throughout the Southern Ocean is regulated by photosynthetic traits. For instance, if
451 the size of the photosynthetic antennae is increased to 2000 Chl : 1 PSII (Strzepek et al., 2019) or
452 reduced to 500 : 1 (Kolber & Falkowski, 1993; Lawrenz et al., 2013), then the overall impact of
453 Mn limitation is decreased or increased by nearly 50%, respectively (Fig. 5).
454

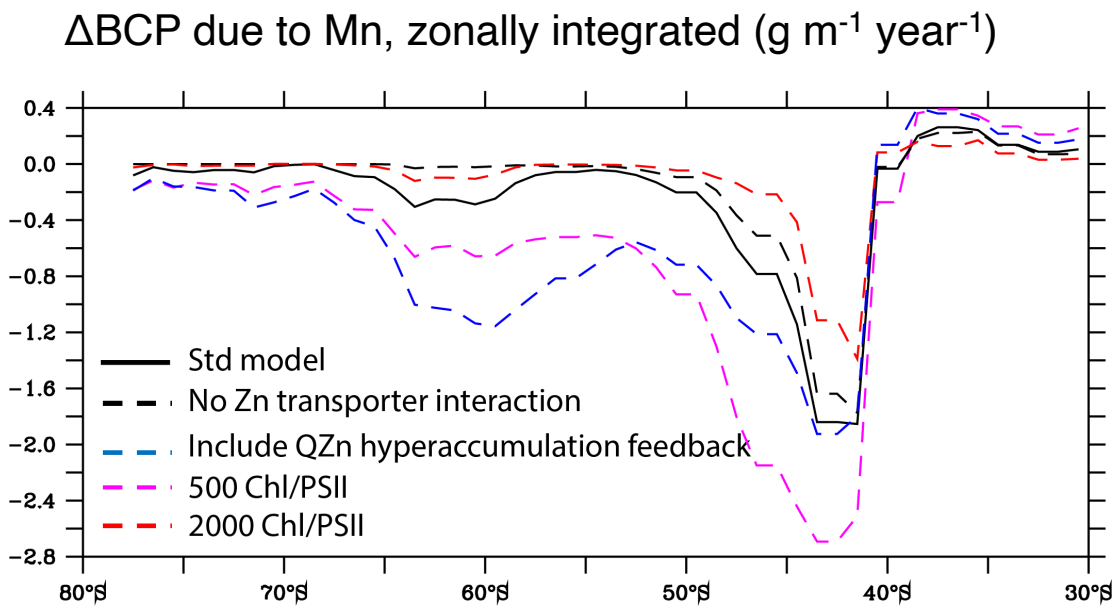

Figure 5. Influence of phytoplankton physiology on the severity of Mn limitation. The zonally integrated anomaly in the Biological Carbon Pump (ΔBCP) at 100 m depth (in grams carbon m^{-1} $year^{-1}$) due to Mn limitation for the PISCES-BYONIC standard model is shown (black line), along with four sensitivity experiments: a model without Zn-Mn transporter competition (black dash), a model with Zn-Mn transporter competition intact and an added downregulation of Mn transport to prevent Zn hyperaccumulation at high Q_{Zn} (blue dash), and the standard model with the upper and lower bounds of the assumed Chl : PSII ratio (red and purple dashes, respectively).

3.5 *Response of Mn limitation to changing iron supply during the Last Glacial Maximum*

The prevalence of Mn deficiency throughout much of the Southern Ocean implies that there is the potential for Mn limitation to become more widespread when Fe supply increases. This is analogous to the Last Glacial Maximum (LGM), when atmospheric dust fluxes to the Southern Ocean were several-fold greater than found today (Lamy et al., 2014; Martin, 1990). In an alternate version of our model without Mn limitation, the biological carbon pump is enhanced throughout the Southern Ocean when atmospheric dust supply is increased following paleo-climate reconstructions (Lambert et al., 2015), as expected (Figure 6a). However, when Mn limitation is considered (Fig. 6b), the increase in the biological carbon pump is stunted by >30% across large regions in the Subantarctic Indian and Pacific sectors (Fig. 6c). Even though the glacial dust scenario increases the supply of both Mn and Fe (indeed dust Mn is much more

476 soluble than Fe in our model; Baker et al., 2013), Mn limitation exceeds Fe limitation throughout
477 the Southern Ocean during spring, with Mn limitation in the Subantarctic Pacific and Indian
478 sectors now persisting through summer (Figure 7). Although these simulations do not consider
479 how parallel changes in ocean circulation may modulate growth conditions in the Southern
480 Ocean, our mechanistic modelling results agree with simpler diagnostic models (Browning et al.,
481 2021) and provide new evidence that Mn was an important influence on the glacial carbon cycle
482 across most of the Southern Ocean. Efforts to reconstruct glacial/ interglacial changes in
483 sedimentary Mn sources, especially from the Antarctic continent, will be essential for refining
484 these conclusions.

485 Earth System Models also project enhanced Southern Ocean productivity by the end of
486 the 21st century due to an increasing Fe supply from the subtropics and the warming and
487 lengthening of the growth season due to sea ice melting (Misumi et al., 2014; Moore et al.,
488 2018). Our simulations suggest that any alleviation of Fe limitation will lead to an expanded
489 impact of Mn deficiency that will add further uncertainty to future projections. This may be
490 particularly important if future warming selects for smaller photosynthetic antennae sizes (as
491 hypothesized in Strzepek et al. (2019)), as our modelling shows that this trait would increase
492 phytoplankton Mn requirements (Fig. 5).
493

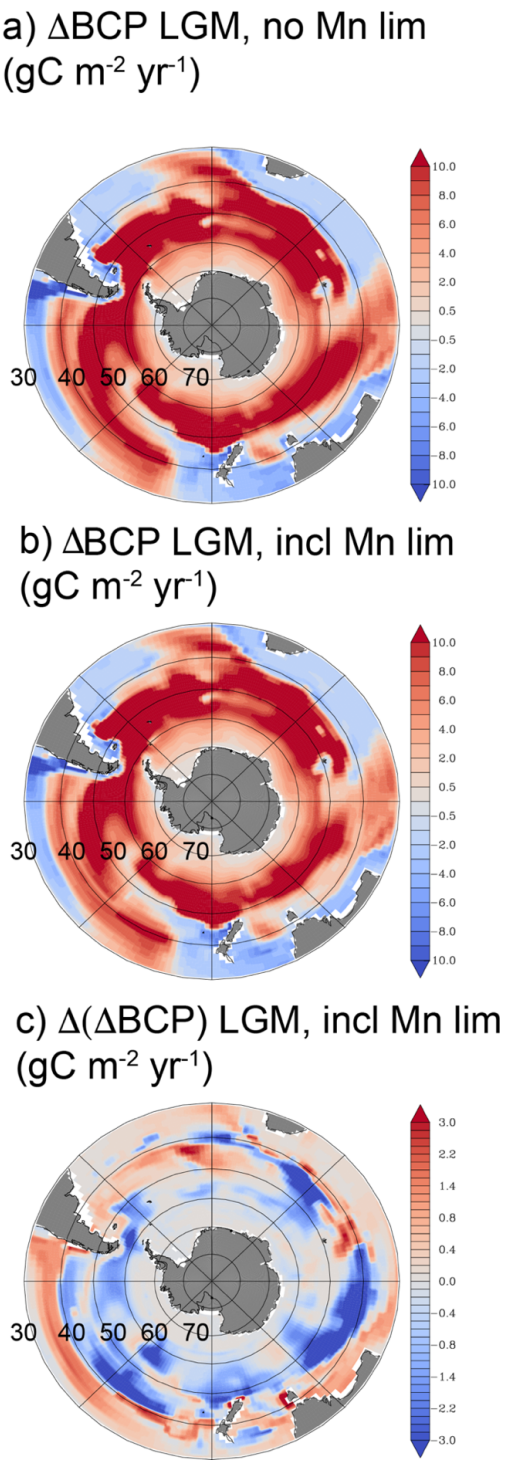

Figure 6. Expansion of Mn limitation with increasing dust supply. The change in the Biological Carbon Pump (ΔBCP) in response to an increase in atmospheric dust supply of both Fe and Mn, based on projections for the Last Glacial Maximum (LGM). Simulation were performed for (a) a model without Mn limitation and (b) the standard PISCES-BYONIC model with Mn limitation feedbacks. The difference (c) shows the impact of Mn on the ΔBCP responses to LGM dust, with blue shading indicating negative anomalies due to Mn limitation. Red areas in panel (c) are those where advection of residual nutrients stimulate the BCP in downstream subtropical regions.

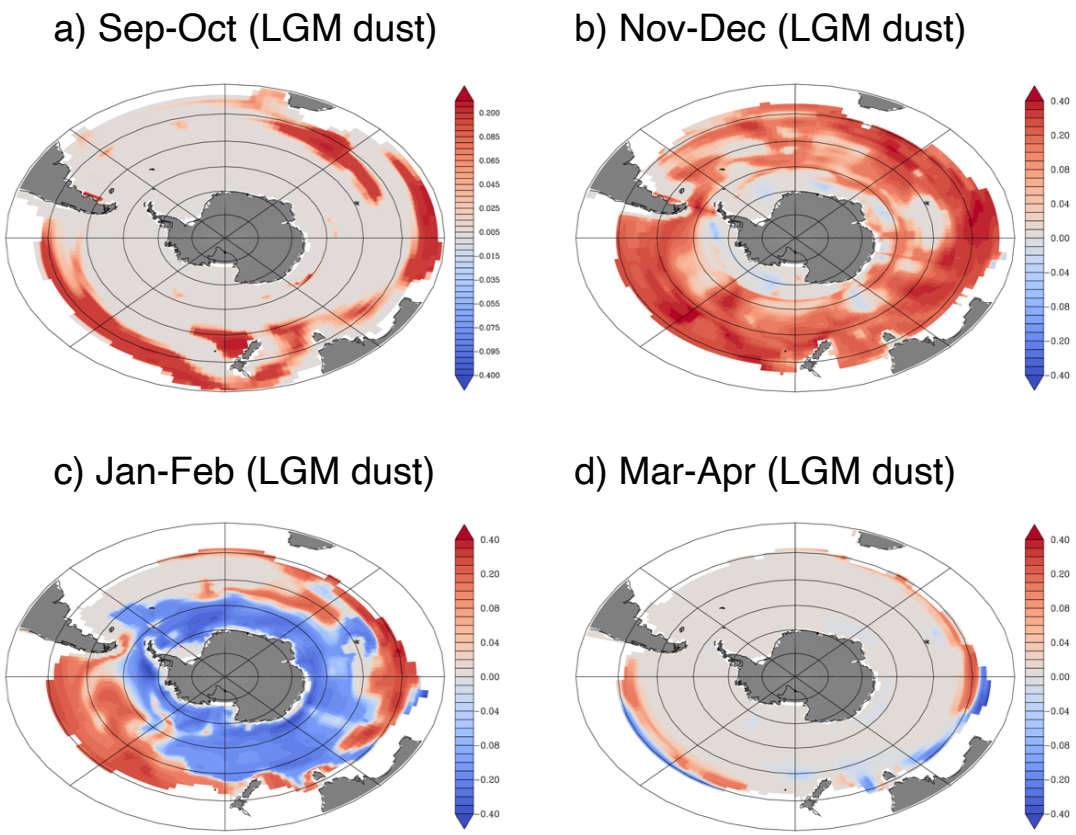

Figure 7. The difference between the fractional Mn limitation and Fe limitation term (normalized across both phytoplankton functional types in the model) for the LGM dust experiment at the ocean surface for (a) September–October, (b) November–December (c) January–February and (d) March–April. Color shading is identical to Figure 4.

4.1 Discussion

We find consistent emergence of phytoplankton Mn limitation under a range of potential physiological adaptations of polar phytoplankton. As a result, projections of past and future changes to Southern Ocean productivity should account for the impact of Mn, alongside the recognized roles of Fe and light. In regions of high Mn supply, the Southern Ocean biological pump oscillates seasonally between light limitation in winter and Fe limitation during summer. Elsewhere, the interaction between light, Mn and Fe will be an important component of the seasonal cycle (Figure 8). Proximal Mn limitation and co-limitation manifests during periods of enhanced Fe availability and sub-optimal light levels, particularly in the Subantarctic zone

during spring. The extent of the light-Mn-Fe co-limited regime over the year (Fig. 8) depends on factors that regulate the demand for PSII (notably traits related to photosynthetic antennae size) or any other process that increases Mn requirements, such as elevated growth rates in response to iron supply or increased expression of Mn superoxide dismutase or other Mn metalloenzymes under Fe limitation (McCain et al., 2021; Peers & Price, 2004). Although our model considers Mn limitation to be independent of any co-occurring Fe deficiency (as in Liebig's Law of the Minimum), protein allocation models suggest that the combined effects of Mn and Fe deficiency might depress growth rates further than singular Fe or Mn limitation (McCain et al., 2021; Pausch et al., 2019; Peers & Price, 2004).

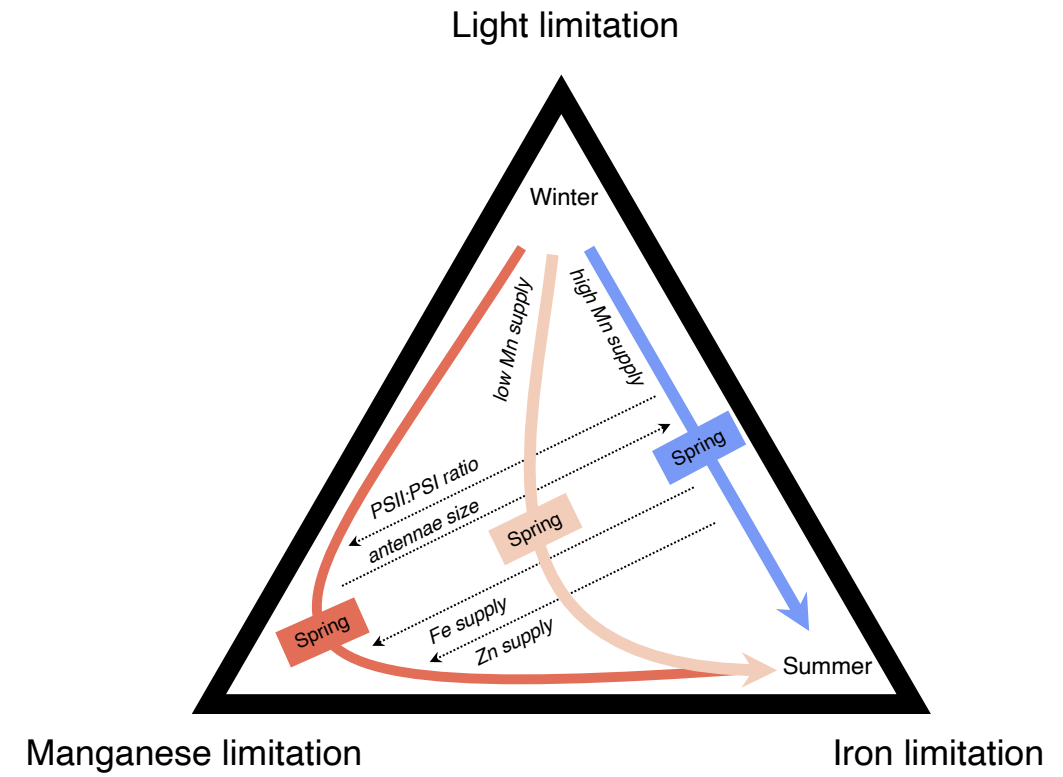

Figure 8. A new perspective on the seasonal transitions between iron, manganese, and light limitation in the Southern Ocean. Under conditions of high Mn supply, the light-Fe limitation seasonal regime is dominant (blue arrow). As Mn supply decreases, a light-Mn-Fe limitation regime manifests (pink and red arrows). The intensity of the Mn-limited component of the light-Mn-Fe limited regime is controlled by photosynthetic physiology (chlorophyll antennae size, PSII:PSI ratio) as well as the supply of Fe and Zn.

In constructing the PISCES-BYONIC model, we have used the limited observational dataset of phytoplankton cell quotas from the Southern Ocean to validate model predictions. Although the model cannot account for the diversity of coexisting phytoplankton species represented in cell-specific Synchrotron X-Ray Fluorescence (SXRF) measurements (Twining, Baines, & Fisher, 2004), simulated cell quotas for Mn, Fe, and Zn follow the same large scale trends found in SXRF datasets (Fig. 2). Modelled Q_{Fe} is several fold greater in the iron-rich North Atlantic compared to the low dFe Southern Ocean (Figure S5), while observed and modelled Q_{Zn} shows the opposite trend: Q_{Zn} peaks in the Antarctic, tracking gradients in dZn (Figs. S2, S6). In contrast, SXRF measurements of Q_{Mn} are relatively similar between the Southern Ocean and North Atlantic, generally falling between 2–5 μmol Mn (mol C)$^{-1}$ (Fig. 2), despite order-of-magnitude differences in dMn between the North Atlantic and the Southern Ocean (Hatta et al., 2015; Latour et al., 2021; Middag et al., 2011). In our model, stabilization of Q_{Mn} is achieved by down-regulating maximum Mn, Fe and Zn uptake rates when metal quotas reach a prescribed maximum and, additionally, when phytoplankton are N-limited. This scheme still allows modelled Q_{Mn} to reach lower values in some Southern Ocean regions than observed by SXRF (Fig. S3), which may reflect the need for broader observational datasets of phytoplankton cell quotas, especially in the Southern Ocean.

The principle uncertainty in our modelling originates from the lack of physiological data for phytoplankton species isolated from the Southern Ocean. Thus far, experiments with Antarctic phytoplankton have focused primarily on responses to Fe and light limitation, and do not include key information associated with Mn uptake and the regulation of Mn transporters (which are described in temperate species, notably *Thalassiosira oceanica* (Sunda & Huntsman, 1986, 2000)). For instance, it is not clear if polar phytoplankton can further optimize their Mn

556 uptake systems, or if improvement is prevented by fundamental constraints on the specificity of
557 Mn^{2+} versus Zn^{2+} binding described by the Irving-Williams series. The modelled footprint of Mn
558 limitation is sensitive to assumptions regarding transporter regulation and photosynthetic
559 antennae size (Fig. 5), but our standard model applies a Chl:PSII ratio that is a relatively good fit
560 with expected Mn requirements of Antarctic phytoplankton (Fig. 1) and also assumes a greater
561 ability to tolerate high Zn than is evident from culture experiments with *T. oceanica*. This
562 suggests that our projections of Mn limitation may be conservative. To accurately project the
563 influence of changing climate on the Southern Ocean biological carbon pump, more culture and
564 field studies focused on Antarctic phytoplankton are required to identify and constrain
565 physiological responses and trade-offs to Mn scarcity.

566 Finally, we note that the ultimate cause of Southern Ocean Mn deficiency – the upwelling
567 of deep ocean waters with high macronutrients and low Mn – has been in place since opening of
568 the Drake Passage and the establishment of the Antarctic circumpolar current during the Eocene
569 (Scher & Martin, 2006). As such, Southern Ocean phytoplankton have had millions of years to
570 adapt to the simultaneous scarcity of Mn, Fe, and light, which may be reflected in their
571 photosynthetic architecture. It is widely thought that selection for Fe-conservation traits alone
572 should lead to high PSII:PSI ratios in Southern Ocean phytoplankton, because Fe is mostly
573 associated with PSI and alternate electron flows that avoid PSI are possible (Behrenfeld &
574 Milligan, 2013; Robert F Strzepek & Harrison, 2004). This strategy is borne out in temperate
575 open-ocean diatom lineages like *T. oceanica*, which show PSII : PSI exceeding 8:1, even when
576 grown under very low irradiance (Strzepek et al., 2019; Strzepek & Harrison, 2004). In this
577 context, the comparatively lower PSII : PSI of ~1.7 (range 1.3 to 2.0) observed in Fe-limited
578 Southern Ocean phytoplankton is enigmatic (Strzepek et al., 2019) because the presence of genes

like plastoquinone terminal oxidase should also allow Antarctic phytoplankton to reach similarly high PSII : PSI ratios (Behrenfeld & Milligan, 2013; Moreno et al., 2018). All photosynthetic Mn is found in PSII, and we estimate that increasing cellular PSII : PSI from 1.7 to 8 could triple photosynthetic Mn requirements relative to Fe (from 0.33 to 1.0 mol Mn : mol Fe; Fig. S7), drastically increasing the susceptibility to Mn limitation in the Mn-deplete Southern Ocean. We posit that the comparatively low PSII : PSI ratios in Southern Ocean phytoplankton may reflect an evolutionary trade-off to optimize photosynthesis in a Southern Ocean that has long been deficient in both Fe and Mn.

Acknowledgments

This work was supported by European Research Council Grant agreement No. 724289 to AT. NJH was supported by Simons Foundation Grant 823167 and BST was supported by National Science Foundation Grants OCE-1829819, OCE-1435862, and OPP-1644155. This research used resources of the Advanced Photon Source, a U.S. Department of Energy (DOE) Office of Science User Facility, operated for the DOE Office of Science by Argonne National Laboratory under Contract No. DE-AC02-06CH11357.

Open Research

Model output from this work will be deposited into Public Repositories (e.g. Zenodo) upon acceptance.

References

Aumont, O., Ethe, C., Tagliabue, A., Bopp, L., & Gehlen, M. (2015). PISCES-v2 : an ocean biogeochemical model for carbon and ecosystme studies. *Geosci. Model Dev.*, *8*, 2465–2513. https://doi.org/10.5194/gmd-8-2465-2015

Baars, O., & Croot, P. L. (2011). The speciation of dissolved zinc in the Atlantic sector of the Southern Ocean. *Deep Sea Research Part II: Topical Studies in Oceanography*, *58*(25), 2720–2732. https://doi.org/https://doi.org/10.1016/j.dsr2.2011.02.003

606 Baars, O., Abouchami, W., Galer, S. J. G., Boye, M., & Croot, P. L. (2014). Dissolved cadmium
607 in the Southern Ocean: Distribution, speciation, and relation to phosphate. *Limnology and*
608 *Oceanography*, *59*(2), 385–399.
609 Baker, A. R., Adams, C., Bell, T. G., Jickells, T. D., & Ganzeveld, L. (2013). Estimation of
610 atmospheric nutrient inputs to the Atlantic Ocean from 50° N to 50° S based on large-scale
611 field sampling: Iron and other dust-associated elements. *Global Biogeochemical Cycles*,
612 *27*(3), 755–767.
613 Behrenfeld, M. J., & Milligan, A. J. (2013). Photophysiological expressions of iron stress in
614 phytoplankton. *Annual Review of Marine Science*, *5*, 217–246.
615 Boyd, P. W. (2002). Environmental factors controlling phytoplankton processes in the Southern
616 Ocean1. *Journal of Phycology*, *38*(5), 844–861.
617 Boyd, P. W., Strzepek, R., Chiswell, S., Chang, H., DeBruyn, J. M., Ellwood, M., et al. (2012).
618 Microbial control of diatom bloom dynamics in the open ocean. *Geophysical Research*
619 *Letters*, *39*(18).
620 Boyle, E. A., Bergquist, B. A., Kayser, R. A., & Mahowald, N. (2005). Iron, manganese, and
621 lead at Hawaii Ocean Time-series station ALOHA: Temporal variability and an
622 intermediate water hydrothermal plume. *Geochimica et Cosmochimica Acta*, *69*(4), 933–
623 952.
624 Browning, T J, Bouman, H. A., Henderson, G. M., Mather, T. A., Pyle, D. M., Schlosser, C., et
625 al. (2014). Strong responses of Southern Ocean phytoplankton communities to volcanic ash.
626 *Geophysical Research Letters*, *41*(8), 2851–2857.
627 Browning, Thomas J, Achterberg, E. P., Engel, A., & Mawji, E. (2021). Manganese co-limitation
628 of phytoplankton growth and major nutrient drawdown in the Southern Ocean. *Nature*

Communications, *12*(1), 884. https://doi.org/10.1038/s41467-021-21122-6

Bucci, V., Nunez-Milland, D., Twining, B. S., & Hellweger, F. L. (2012). Microscale patchiness leads to large and important intraspecific internal nutrient heterogeneity in phytoplankton. *Aquatic Ecology*, *46*(1), 101–118.

Buma, A. G. J., De Baar, H. J. W., Nolting, R. F., & Van Bennekom, A. J. (1991). Metal enrichment experiments in the Weddell-Scotia Seas: Effects of iron and manganese on various plankton communities. *Limnology and Oceanography*, *36*(8), 1865–1878.

Droop, M. R. (1973). Some thoughts on nutrient limitation in algae. *Journal of Phycology*. https://doi.org/10.1111/j.1529-8817.1973.tb04092.x

Ellwood, M. J., Strzepek, R. F., Strutton, P. G., Trull, T. W., Fourquez, M., & Boyd, P. W. (2020). Distinct iron cycling in a Southern Ocean eddy. *Nature Communications*, *11*(1), 1–8.

Geider, R. J., MacIntyre, H. L., & Kana, T. M. (1997). Dynamic model of phytoplankton growth and acclimation: responses of the balanced growth rate and the chlorophyll a: carbon ratio to light, nutrient-limitation and temperature. *Marine Ecology Progress Series*, *148*, 187–200.

Hatta, M., Measures, C. I., Wu, J., Roshan, S., Fitzsimmons, J. N., Sedwick, P., & Morton, P. (2015). An overview of dissolved Fe and Mn distributions during the 2010–2011 US GEOTRACES north Atlantic cruises: GEOTRACES GA03. *Deep Sea Research Part II: Topical Studies in Oceanography*, *116*, 117–129.

Heller, M. I., & Croot, P. L. (2015). Copper speciation and distribution in the Atlantic sector of the Southern Ocean. *Marine Chemistry*, *173*, 253–268.

Hulten, M. van, Middag, R., Dutay, J.-C., Baar, H. de, Roy-Barman, M., Gehlen, M., et al.

(2017). Manganese in the west Atlantic Ocean in the context of the first global ocean circulation model of manganese. *Biogeosciences*, *14*(5), 1123–1152.

Irving, H., & Williams, Rjp. (1953). 637. The stability of transition-metal complexes. *Journal of the Chemical Society (Resumed)*, 3192–3210.

Jaccard, S. L., Hayes, C. T., Martinez-Garcia, A., Hodell, D. A., Anderson, R. F., Sigman, D. M., & Haug, G. H. (2013). Two modes of change in Southern Ocean productivity over the past million years. *Science*, *339*(6126), 1419–1423.

Jensen, E. L., Clement, R., Kosta, A., Maberly, S. C., & Gontero, B. (2019). A new widespread subclass of carbonic anhydrase in marine phytoplankton. *The ISME Journal*, *13*(8), 2094–2106.

Johnson, K. S., Coale, K. H., Berelson, W. M., & Michael Gordon, R. (1996). On the formation of the manganese maximum in the oxygen minimum. *Geochimica et Cosmochimica Acta*, *60*(8), 1291–1299. https://doi.org/10.1016/0016-7037(96)00005-1

Kolber, Z., & Falkowski, P. G. (1993). Use of active fluorescence to estimate phytoplankton photosynthesis in situ. *Limnology and Oceanography*, *38*(8), 1646–1665.

Lambert, F., Tagliabue, A., Shaffer, G., Lamy, F., Winckler, G., Farias, L., et al. (2015). Dust fluxes and iron fertilization in Holocene and Last Glacial Maximum climates. *Geophysical Research Letters*, *42*(14), 6014–6023.

Lamy, F., Gersonde, R., Winckler, G., Esper, O., Jaeschke, A., Kuhn, G., et al. (2014). Increased dust deposition in the Pacific Southern Ocean during glacial periods. *Science*, *343*(6169), 403–407.

Landing, W. M., & Bruland, K. W. (1987). The contrasting biogeochemistry of iron and manganese in the Pacific Ocean. *Geochimica et Cosmochimica Acta*, *51*(1), 29–43.

675 Latour, P., Wuttig, K., van Der Merwe, P., Strzepek, R. F., Gault-Ringold, M., Townsend, A. T.,
676 et al. (2021). Manganese biogeochemistry in the Southern Ocean, from Tasmania to
677 Antarctica. *Limnology and Oceanography*.
678 Lawrenz, E., Silsbe, G., Capuzzo, E., Ylöstalo, P., Forster, R. M., Simis, S. G. H., et al. (2013).
679 Predicting the electron requirement for carbon fixation in seas and oceans. *PloS One*, *8*(3),
680 e58137.
681 Martin, J. H. (1990). Glacial-interglacial CO2 change: The iron hypothesis. *Paleoceanography*,
682 *5*(1), 1–13.
683 Martin, J. H., Fitzwater, S. E., & Gordon, R. M. (1990). Iron deficiency limits phytoplankton
684 growth in Antarctic waters. *Global Biogeochemical Cycles*, *4*(1), 5–12.
685 Martin, J. H., Gordon, R. M., & Fitzwater, S. E. (1990). Iron in Antarctic waters. *Nature*,
686 *345*(6271), 156–158.
687 Martínez-García, A., Sigman, D. M., Ren, H., Anderson, R. F., Straub, M., Hodell, D. A., et al.
688 (2014). Iron fertilization of the Subantarctic Ocean during the last ice age. *Science*,
689 *343*(6177), 1347–1350.
690 McCain, J. S. P., Tagliabue, A., Susko, E., Achterberg, E. P., Allen, A. E., & Bertrand, E. M.
691 (2021). Cellular costs underpin micronutrient limitation in phytoplankton. *Science*
692 *Advances*, *7*(32), eabg6501. https://doi.org/10.1126/sciadv.abg6501
693 Middag, R d, De Baar, H. J. W., Laan, P., Cai, P. H. v, & Van Ooijen, J. C. (2011). Dissolved
694 manganese in the Atlantic sector of the Southern Ocean. *Deep Sea Research Part II:*
695 *Topical Studies in Oceanography*, *58*(25–26), 2661–2677.
696 Middag, Rob, de Baar, H. J. W., Klunder, M. B., & Laan, P. (2013). Fluxes of dissolved
697 aluminum and manganese to the Weddell Sea and indications for manganese co-limitation.

Limnology and Oceanography, *58*(1), 287–300.

Misumi, K., Lindsay, K., Moore, J. K., Doney, S. C., Bryan, F. O., Tsumune, D., & Yoshida, Y. (2014). The iron budget in ocean surface waters in the 20th and 21st centuries: projections by the Community Earth System Model version 1. *Biogeosciences*, *11*(1), 33–55.

Moore, C. M. (2016). Diagnosing oceanic nutrient deficiency. *Philosophical Transactions of the Royal Society A: Mathematical, Physical and Engineering Sciences*, *374*(2081), 20150290.

Moore, J. K., Fu, W., Primeau, F., Britten, G. L., Lindsay, K., Long, M., et al. (2018). Sustained climate warming drives declining marine biological productivity. *Science*, *359*(6380), 1139 LP – 1143. Retrieved from http://science.sciencemag.org/content/359/6380/1139.abstract

Moreno, C. M., Lin, Y., Davies, S., Monbureau, E., Cassar, N., & Marchetti, A. (2018). Examination of gene repertoires and physiological responses to iron and light limitation in Southern Ocean diatoms. *Polar Biology*, *41*(4), 679–696.

Pausch, F., Bischof, K., & Trimborn, S. (2019). Iron and manganese co-limit growth of the Southern Ocean diatom Chaetoceros debilis. *PLoS One*, *14*(9), e0221959.

Peers, G., & Price, N. M. (2004). A role for manganese in superoxide dismutases and growth of iron-deficient diatoms. *Limnology and Oceanography*, *49*(5), 1774–1783.

Raven, J. A. (1988). The iron and molybdenum use efficiencies of plant growth with different energy, carbon and nitrogen sources. *New Phytologist*, *109*(3), 279–288. https://doi.org/10.1111/j.1469-8137.1988.tb04196.x

Raven, J. A. (1990). Predictions of Mn and Fe use efficiencies of phototrophic growth as a function of light availability for growth and of C assimilation pathway. *New Phytologist*, *116*(1), 1–18. https://doi.org/10.1111/j.1469-8137.1990.tb00505.x

Resing, J. A., Sedwick, P. N., German, C. R., Jenkins, W. J., Moffett, J. W., Sohst, B. M., &

721 Tagliabue, A. (2015). Basin-scale transport of hydrothermal dissolved metals across the
722 South Pacific Ocean. *Nature*, *523*(7559), 200.
723 Richon, C., & Tagliabue, A. (2019). Insights into the major processes driving the global
724 distribution of copper in the ocean from a global model. *Global Biogeochemical Cycles*,
725 *33*(12), 1594–1610.
726 Richon, C., & Tagliabue, A. (2021). Biogeochemical feedbacks associated with the response of
727 micronutrient recycling by zooplankton to climate change. *Global Change Biology*.
728 Rigby, S. J., Williams, R. G., Achterberg, E. P., & Tagliabue, A. (2020). Resource availability
729 and entrainment are driven by offsets between nutriclines and winter mixed-layer depth.
730 *Global Biogeochemical Cycles*, *34*(7), e2019GB006497.
731 Sarmiento, J. L., & Toggweiler, J. R. (1984). A new model for the role of the oceans in
732 determining atmospheric pCO2. *Nature*, *308*(5960), 621–624.
733 Sarmiento, J. L., Gruber, N., Brzezinski, M. A., & Dunne, J. P. (2004). High-latitude controls of
734 thermocline nutrients and low latitude biological productivity. *Nature*, *427*(6969), 56–60.
735 Scher, H. D., & Martin, E. E. (2006). Timing and climatic consequences of the opening of Drake
736 Passage. *Science*, *312*(5772), 428–430.
737 Sigman, D. M., & Boyle, E. A. (2000). Glacial/interglacial variations in atmospheric carbon
738 dioxide. *Nature*, *407*(6806), 859.
739 Sigman, D. M., Hain, M. P., & Haug, G. H. (2010). The polar ocean and glacial cycles in
740 atmospheric CO 2 concentration. *Nature*, *466*(7302), 47–55.
741 Strzepek, R F, Maldonado, M. T., Higgins, J. L., Hall, J., Safi, K., Wilhelm, S. W., & Boyd, P.
742 W. (2005). Spinning the “Ferrous Wheel”: The importance of the microbial community in
743 an iron budget during the FeCycle experiment. *Global Biogeochemical Cycles*, *19*(4).

744 Strzepek, Robert F, & Harrison, P. J. (2004). Photosynthetic architecture differs in coastal and
745 oceanic diatoms. *Nature*, *431*(7009), 689–692.
746 Strzepek, Robert F, Boyd, P. W., & Sunda, W. G. (2019). Photosynthetic adaptation to low iron,
747 light, and temperature in Southern Ocean phytoplankton. *Proceedings of the National*
748 *Academy of Sciences*, *116*(10), 4388–4393.
749 Sunda, W. G. (1989). Trace metal interactions with marine phytoplankton. *Biological*
750 *Oceanography*, *6*(5–6), 411–442.
751 Sunda, W. G., & Huntsman, S. a. (1988). Effect of sunlight on redox cycles of manganese in the
752 southwestern Sargasso Sea. *Deep Sea Research Part A. Oceanographic Research Papers*,
753 *35*(8), 1297–1317. https://doi.org/10.1016/0198-0149(88)90084-2
754 Sunda, W. G., & Huntsman, S. A. (1983). Effect of competitive interactions between manganese
755 and copper on cellular manganese and growth in estuarine and oceanic species of the diatom
756 Thalassiosira 1, 2. *Limnology and Oceanography*, *28*(5), 924–934.
757 Sunda, W. G., & Huntsman, S. A. (1986). RELATIONSHIPS AMONG GROWTH RATE,
758 CELLULAR MANGANESE CONCENTRATIONS AND MANGANESE TRANSPORT
759 KINETICS IN ESTUARINE AND OCEANIC SPECIES OF THE DIATOM
760 THALASSIODIRA 1. *Journal of Phycology*, *22*(3), 259–270.
761 Sunda, W. G., & Huntsman, S. A. (1995a). Cobalt and zinc interreplacement in marine
762 phytoplankton: Biological and geochemical implications. *Limnology and Oceanography*,
763 *40*(8), 1404–1417. https://doi.org/10.4319/lo.1995.40.8.1404
764 Sunda, W. G., & Huntsman, S. A. (1995b). Iron uptake and growth limitation in oceanic and
765 coastal phytoplankton. *Marine Chemistry*, *50*(1–4), 189–206. https://doi.org/10.1016/0304-
766 4203(95)00035-P

767 Sunda, W. G., & Huntsman, S. A. (1996). Antagonisms between cadmium and zinc toxicity and
768 manganese limitation in a coastal diatom. *Limnology and Oceanography*, *41*(3), 373–387.
769 Sunda, W. G., & Huntsman, S. A. (1998a). Interactions among Cu2+, Zn2+, and Mn2+ in
770 controlling cellular Mn, Zn, and growth rate in the coastal alga Chlamydomonas. *Limnology*
771 *and Oceanography*, *43*(6), 1055–1064.
772 Sunda, W. G., & Huntsman, S. A. (1998b). Interactive effects of external manganese, the toxic
773 metals copper and zinc, and light in controlling cellular manganese and growth in a coastal
774 diatom. *Limnology and Oceanography*, *43*(7), 1467–1475.
775 Sunda, W. G., & Huntsman, S. A. (2000). Effect of Zn, Mn, and Fe on Cd accumulation in
776 phytoplankton: implications for oceanic Cd cycling. *Limnology and Oceanography*, *45*(7),
777 1501–1516.
778 Tagliabue, A., & Resing, J. (2016). Impact of hydrothermalism on the ocean iron cycle.
779 *Philosophical Transactions of the Royal Society A: Mathematical, Physical and*
780 *Engineering Sciences*, *374*(2081), 20150291.
781 Tagliabue, A., Sallée, J.-B., Bowie, A. R., Lévy, M., Swart, S., & Boyd, P. W. (2014). Surface-
782 water iron supplies in the Southern Ocean sustained by deep winter mixing. *Nature*
783 *Geoscience*, *7*(4), 314–320.
784 Tagliabue, A., Aumont, O., DeAth, R., Dunne, J. P., Dutkiewicz, S., Galbraith, E., et al. (2016).
785 How well do global ocean biogeochemistry models simulate dissolved iron distributions?
786 *Global Biogeochemical Cycles*, *30*(2), 149–174.
787 Tagliabue, A., Bowie, A. R., Boyd, P. W., Buck, K. N., Johnson, K. S., & Saito, M. A. (2017).
788 The integral role of iron in ocean biogeochemistry. *Nature*, *543*(7643), 51–59.
789 Tagliabue, A., Hawco, N. J., Bundy, R. M., Landing, W. M., Milne, A., Morton, P. L., & Saito,

M. A. (2018). The Role of External Inputs and Internal Cycling in Shaping the Global Ocean Cobalt Distribution: Insights From the First Cobalt Biogeochemical Model. *Global Biogeochemical Cycles*, *32*(4), 594–616. https://doi.org/10.1002/2017GB005830

Twining, B. S., & Baines, S. B. (2013). The trace metal composition of marine phytoplankton. *Annual Review of Marine Science*, *5*, 191–215.

Twining, B. S., Baines, S. B., Fisher, N. S., & Landry, M. R. (2004). Cellular iron contents of plankton during the Southern Ocean Iron Experiment (SOFeX). *Deep Sea Research Part I: Oceanographic Research Papers*, *51*(12), 1827–1850.

Twining, B. S., Baines, S. B., & Fisher, N. S. (2004). Element stoichiometries of individual plankton cells collected during the Southern Ocean Iron Experiment (SOFeX). *Limnology and Oceanography*, *49*(6), 2115–2128.

Twining, B. S., Baines, S. B., Bozard, J. B., Vogt, S., Walker, E. a., & Nelson, D. M. (2011). Metal quotas of plankton in the equatorial Pacific Ocean. *Deep Sea Research Part II: Topical Studies in Oceanography*, *58*(3–4), 325–341. https://doi.org/10.1016/j.dsr2.2010.08.018

Twining, B. S., Rauschenberg, S., Baer, S. E., Lomas, M. W., Martiny, A. C., & Antipova, O. (2019). A nutrient limitation mosaic in the eastern tropical Indian Ocean. *Deep Sea Research Part II: Topical Studies in Oceanography*, *166*, 125–140.

Twining, B. S., Antipova, O., Chappell, P. D., Cohen, N. R., Jacquot, J. E., Mann, E. L., et al. (2020). Taxonomic and nutrient controls on phytoplankton iron quotas in the ocean. *Limnology and Oceanography Letters*.

Waldron, K. J., & Robinson, N. J. (2009). How do bacterial cells ensure that metalloproteins get the correct metal? *Nature Reviews Microbiology*, *7*(1), 25–35.

Weber, T., John, S., Tagliabue, A., & DeVries, T. (2018). Biological uptake and reversible scavenging of zinc in the global ocean. *Science*, *361*(6397), 72–76.

Wu, M., McCain, J. S. P., Rowland, E., Middag, R., Sandgren, M., Allen, A. E., & Bertrand, E. M. (2019). Manganese and iron deficiency in Southern Ocean Phaeocystis antarctica populations revealed through taxon-specific protein indicators. *Nature Communications*, *10*(1), 1–10.